P9.10 INTERPRETATION OF SIMULATED WSR-88D DOPPLER VELOCITY SIGNATURES OF TORNADOES ASSOCIATED WITH NONUNIFORM REFLECTIVITIES

Rodger A. Brown and Vincent T. Wood
NOAA/National Severe Storms Laboratory, Norman, OK

David C. Dowell
National Center for Atmospheric Research, Boulder, CO

1. INTRODUCTION

Weather radars located within 10–20 km of a significant tornado reveal the presence of a weak reflectivity "eye" centered on the tornado (e.g., Fujita and Wakimoto 1982; Wakimoto and Martner 1992; Wurman et al. 1996: Wakimoto et al. 1996; Wurman and Gill 2000; Bluestein and Pazmany 2000; Wakimoto et al. 2003; Bluestein et al. 2003; Bluestein et al. 2004; Alexander and Wurman, 2005). The eye results from the centrifuging of debris and hydrometeors by the strong rotating winds within the tornado. At other times, when radar measurements are made close to the ground or at significant distances from the radar, a reflectivity maximum, or "knob," is centered on the tornado. Wood et al. (2005) investigated the situations where eyes and knobs appear using simulated WSR-88D radar measurements in numerically modeled tornadoes.

Since a Doppler velocity value is the reflectivity-weighted mean of the radial motion of all the radar scatterers within the radar beam, a nonuniform distribution of scatterers will produce a different mean Doppler velocity value than will a uniform distribution of scatterers. If all of the scatterers are the same size (i.e., having the same reflectivity value), the computed mean Doppler velocity value is a true representation of the mean radial component of scatterer motion within the beam. However, nonuniform reflectivities across the beam will bias the indicated size and strength of the tornado's core region within the radius of peak tangential velocities.

In this paper, we compare the effects of uniform and nonuniform drop size distributions (reflectivities) on the deduced sizes and strengths of three numerically modeled tornadoes using a simulated WSR-88D.

2. METHOD

a. Numerical tornado model

We used the Dowell et al. (2005) two-dimensional (radius versus height) numerical model to conduct three experiments, each simulating a different sized tornado. The model consisted of axisymmetric forced convection (buoyant bubble along the central axis) inside a closed impermeable cylinder that rotated with a constant angular velocity. As the central updraft developed, air converging into the lower portion of the domain experienced an increase in tangential velocity, leading to the development of a tornado. In this way, a fully three-dimensional flow field developed consisting of evolving radial, vertical, and tangential velocity components.

The model permits objects (debris and hydrometeors) to be moved and centrifuged by the flow field. Each sized object has its own specified terminal fall velocity. We chose to include only hydrometeors in our experiments. However, the sizes of hydrometeors within tornadoes are not known. After experimenting with various sized raindrops, we found that the centrifuging of 1.5 mm diameter drops (terminal fall velocity of 5.4 m s^{-1}) produced realistic weak-reflectivity eyes. From their experiments, Dowell et al. (2005) deduced that raindrops with fall velocities less than 10 m s^{-1} likely are the dominant radar scatterers within tornadoes.

In addition to the nonuniform reflectivity field produced by the numerical model, we used a uniform reflectivity version where the three-dimensional flow field produced by the model also was used, but the reflectivity field was assumed to be uniform and was computed from the initial raindrop concentration in the model. The constant value of the resulting reflectivity field was 20 dBZ.

b. Doppler radar emulator

WSR-88D Doppler velocity measurements in the model tornadoes were simulated using a Doppler radar emulator that reproduced the basic characteristics of a WSR-88D, but several simplifications were employed. Instead of the radar beam consisting of a main lobe and side lobes, it consisted only of a main lobe that was represented by a Gaussian distribution having a width of three half-power beamwidths. Doppler velocity values were computed from the Doppler component of the three-dimensional model raindrop motion. Rather than computing mean Doppler velocity and reflectivity values from a given number of pulses, the values were computed from Gaussian-weighted model Doppler velocity and reflectivity values within the radar beam. To compensate for antenna rotation in the azimuthal direction during the time it takes to collect the required number of samples, the horizontal dimension of the beam was represented by a broadened *effective* half-power beamwidth. The effective half-power beamwidth is specified by the azimuthal sampling interval, which in turn is specified by the number of pulses, pulse

Corresponding author address: Dr. Rodger A. Brown, National Severe Storms Laboratory, 120 David L. Boren Blvd., Norman, OK 73072. E-mail: Rodger.Brown @noaa.gov

repetition frequency, and antenna rotation rate (e.g., Doviak and Zrnić 1993; pp. 193–197).

Doppler radar data were simulated using two different spatial resolutions: (1) current resolution and (2) super resolution. WSR-88Ds currently process and display data at 1.0^{o} azimuthal intervals; the range interval for reflectivity is 1.0 km and for Doppler velocity is 0.25 km. Wood et al. (2001) and Brown et al. (2002) showed through simulations that WSR-88D detections of mesocyclones and tornadoes, respectively, could be improved by collecting finer-resolution—now called super-resolution—data. For super-resolution data collection, both Doppler velocity and reflectivity data are processed at 0.5^{o} azimuthal and 0.25 km range intervals. Brown et al. (2005) used the National Severe Storms Laboratory's test bed WSR-88D (KOUN) to show that actual reflectivity and Doppler velocity signatures in severe storms are more clearly depicted with super-resolution data. The capability to process super-resolution data at lower elevation angles is scheduled to be added to WSR-88Ds in the 2008–2009 time frame.

3. RESULTS

Three different tornadoes were created using the numerical tornado model. In Experiment I (EXP I), a medium-sized tornado was produced. Several attempts were made to form a smaller tornado that had a core diameter in the 50–100 m category by varying the model's input parameters. However, the attempts were unsuccessful. Instead, we settled for a tornado that had a core diameter aloft of 150 m and peak tangential velocity of 32 m s^{-1}. In Experiment II (EXP II), a large tornado having a core diameter aloft of 326 m and peak tangential velocity of 62 m s^{-1} was produced and in Experiment III (EXP III) a rare very large tornado having a core diameter aloft of 676 m and peak tangential velocity of 64 m s^{-1} was produced.

Examples of simulated Doppler velocity and reflectivity profiles in the radial direction from the centers of the three model tornadoes for the two Doppler radar data resolutions are shown in Figs. 1–3. The data are presented at a height of 1.0 km and at a variety of ranges from the simulated radar. Each panel in the figures consists of three pairs of curves representing (1) tangential velocity of the model raindrops and reflectivity computed directly from the model raindrop concentrations, (2) WSR–88D Doppler velocity and reflectivity measurements computed from the model tangential velocity and model reflectivity (nonuniform) values, and (3) WSR–88D Doppler velocity and reflectivity measurements based on model tangential velocity values and a uniform reflectivity value of 20 dBZ that represents the initial concentration of raindrops in the model.

It may be noted in Figs. 1–3 that, owing to the widening radar beam with increasing range, the peak Doppler velocity values in each experiment decrease and the distance of the peak from the tornado center increases with increasing range. In addition, the weak reflectivity eye and surrounding stronger reflectivity annulus changes into a nearly flat reflectivity profile with a slight maximum centered on the tornado (e.g., Wood et al. 2005). The widening beam with range is represented by the ratio of effective beamwidth to tornado core diameter (EBW/CD) indicated at the top of each panel.

When the beam is much smaller than the tornado (e.g., Fig. 3a), Doppler velocity and reflectivity measurements faithfully reproduce the tangential velocity and reflectivity values in the tornado. As the beam widens with increasing range, the resulting Doppler velocity profile is affected differently depending on the model reflectivity profile. For the uniform reflectivity model, the associated Doppler velocity values (blue dashed line with dots) initially do not depart much from the tangential velocity values (e.g., Fig. 3c).

However, when the beamwidth is generally less than the core diameter (e.g., Figs. 2a–2d, 3c–3f), the nonuniform reflectivity model results in a Doppler velocity profile (red line with dots) that peaks closer to the tornado center than does the tangential velocity profile (black line). The peak occurring closer to the tornado center is a consequence of the fact that the mean Doppler velocity value within the beam is weighted by both the distribution of reflectivity values within the beam and the Gaussian shape of the beam itself. Near the center of the tornado, reflectivity is very weak owing to the centrifuging of raindrops. Consequently, when the radar beam is slightly offset from the tornado center, the only tangential velocity values within the beam that have significant reflectivity values are found at the edge of the beam near the peak of the tangential velocity profile. The radar processor places the mean Doppler velocity value at the center of the beam even though the only tangential velocity values having significant reflectivity values are located on one side of the beam.

As the beamwidth becomes significantly wider than the tornado's core diameter, the peaks of the Doppler velocity curves decrease in magnitude and move father away from the tornado center. In the limit, the Doppler velocity curves based on uniform and nonuniform reflectivity profiles approach each other and continue to weaken, while the nonuniform Doppler reflectivity curve approaches the constant 20 dBZ value of the uniform profile (e.g., Figs. 1d–1f, 2f–2h, 3h).

The panels in Figs. 1–3 also show the advantage of WSR–88D super-resolution sampling ($\Delta AZ = 0.5^{o}$) over current-resolution sampling ($\Delta AZ = 1.0^{o}$). With 0.5^{o} sampling, there is less degradation of the Doppler velocity and reflectivity profiles because the effective beamwidth is narrower (e.g., Brown et al. 2005).

4. DISCUSSION

As a first approximation when computing simulated Doppler velocity values across a tornado, one assumes that the reflectivity is constant. However, mobile Doppler radar measurements made in the immediate vicinity of tornadoes show the presence of a pronounced reflectivity minimum that extends across most of the core region. Since the minimum is produced by the centrifuging of hydrometeors, we used the numerical model of Dowell et al. (2005) to simulate

realistic three-dimensional flow around an axisymmetric tornado. Sampling of the model flow field and centrifuged hydrometeors by a simulated WSR–88D produced Doppler velocity and nonuniform reflectivity fields that could be compared with Doppler velocity fields associated with the model flow field and assumed uniform reflectivities across the tornado.

For both the uniform and nonuniform reflectivity fields, the peak Doppler velocities decreased in magnitude and the apparent core diameter increased with increasing distance from the radar (i.e., with increasing beamwidth). At the same time, the uniform reflectivity field did not change but the nonuniform reflectivity eye filled with increasing range and approached the uniform reflectivity value when beamwidths were greater than about two core diameters.

With the presence of the weak reflectivity eye at the center of the tornado, nearby Doppler velocity measurements (i.e., EBW/CD less than about one) had a peak velocity that was significantly closer to the tornado center than seen in the model tangential velocity field. This distorted Doppler velocity profile was due to radar beams positioned within the core region having negligible reflectivity-weighted Doppler velocity values within the eye. Consequently, the only Doppler velocity values being averaged were those strong ones in the part of the beam at the edge of the core region. *Therefore one can expect the Doppler-indicated radius of peak wind to underestimate the true radius when the effective beamwidth is less than the tornado's core diameter and there is a weak reflectivity eye at the center of the tornado.*

At a given range from a WSR-88D, the simulations show that super-resolution data ($\Delta AZ = 0.5^o$) produce less degraded Doppler velocity and reflectivity signatures of tornadoes than do the current-resolution data ($\Delta AZ = 1.0^o$). This finding is supported by test bed WSR-88D measurements in tornadoes and mesocyclones (e.g., Brown et al. 2005). Forecasters will be able to benefit from the improved detection capability of super-resolution data by about 2009.

Acknowledgments. Development of the numerical vortex model used in this study was supported by the National Science Foundation under Grant No. 0437898.

5. REFERENCES

Alexander, C. R., and J. Wurman, 2005: The 30 May 1998 Spencer, South Dakota, storm. Part I: The structural evolution and environment of the tornadoes. *Mon. Wea. Rev*., **133**, 72–96.

Bluestein, H. B., and A. L. Pazmany, 2000: Observations of tornadoes and other convective phenomena with a mobile, 3-mm wavelength, Doppler radar: The Spring 1999 field experiment. *Bull. Amer. Meteor. Soc*., **81**, 2939–2951.

_____, C. C. Weiss, and A. L. Pazmany, 2004: The vertical structure of a tornado near Happy, Texas, on 5 May 2002: High-resolution, mobile, W-band, Doppler radar observations. *Mon. Wea. Rev*., **132**, 2325–2337.

_____, W.-C. Lee, M. Bell, C. C. Weiss, and A. L. Pazmany, 2003: Mobile Doppler radar observations of a tornado in a supercell near Bassett, Nebraska, on 5 June 1999. Part II: Tornado-vortex structure. *Mon. Wea. Rev*., **131**, 2968–2984.

Brown, R. A., V. T. Wood, and D. Sirmans, 2002: Improved tornado detection using simulated and actual WSR-88D data with enhanced resolution. *J. Atmos. Oceanic Technol*., **19**, 1759–1771.

_____, B. A. Flickinger, E. Forren, D. M. Schultz, D. Sirmans, P. L. Spencer, V. T. Wood, and C. L. Ziegler, 2005: Improved detection of severe storms using experimental fine-resolution WSR-88D measurements. *Wea. Forecasting*, **20**, 3–14.

Doviak, R. J., and D. S. Zrnić, 1993: *Doppler Radar and Weather Observations*. 2nd ed., Academic Press, 562 pp.

Dowell, D. C., C. R. Alexander, J. M. Wurman, and L. J. Wicker, 2005: Centrifuging of hydrometeors and debris in tornadoes: Radar-reflectivity patterns and wind-measurement errors. *Mon. Wea. Rev*., **133**, 1501–1524.

Fujita, T. T., and R. M. Wakimoto, 1982: Anticyclonic tornadoes in 1980 and 1981. Preprints, *12th Conf. on Severe Local Storms*, Amer. Meteor. Soc., San Antonio, TX, 401–404.

Wakimoto, R. M., and B. E. Martner, 1992: Observations of a Colorado tornado. Part II: Combined photogrammetric and Doppler radar analysis. *Mon. Wea. Rev*., **120**, 522–543.

_____, W.-C. Lee, H. B. Bluestein, C.-H. Liu, and P. H. Hildebrand, 1996: ELDORA observations during VORTEX 95. *Bull. Amer. Meteor. Soc*., **77**, 1465–1481.

_____, H. V. Murphey, D. C. Dowell, and H. B. Bluestein, 2003: The Kellerville tornado during VORTEX: Damage survey and Doppler radar analysis. *Mon. Wea. Rev*., **131**, 2197–2221.

Wood, V. T., R. A. Brown, and D. Sirmans, 2001: Technique for improving detection of WSR-88D mesocyclone signatures by increasing angular sampling. *Wea. Forecasting*, **16**, 177–184.

_____, _____, and D. C. Dowell, 2005: Simulated WSR-88D measurements of low-reflectivity eyes associated with tornadoes. *Preprints*, 32nd Conf. on Radar Meteor., Albuquer-que, Amer. Meteor. Soc., CD-ROM, P15R.6.

Wurman, J., and S. Gill, 2000: Finescale radar observations of the Dimmitt, Texas (2 June 1995), tornado. *Mon. Wea. Rev*., **128**, 2135–2164.

_____, J. M. Straka, and E. N. Rasmussen, 1996: Fine-scale Doppler radar observations of tornadoes. *Science*, **272**, 1774–1777.

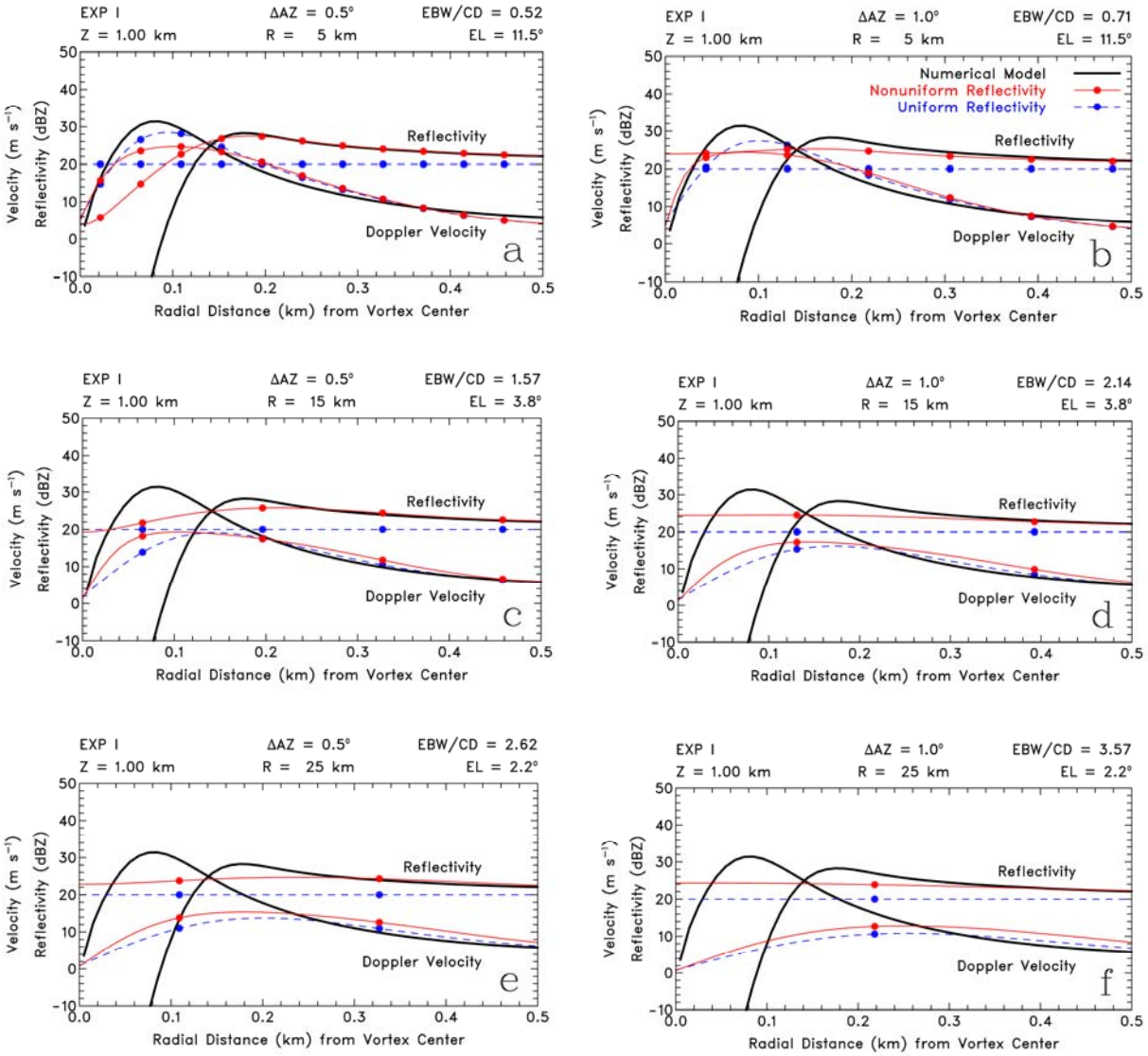

Fig. 1. Radial profiles of velocity and reflectivity for Experiment I at a height of 1 km and ranges of 5, 15, and 25 km from the simulated radar. The black curves represent radial profiles of the tangential velocity of the model raindrops and the reflectivity computed directly from the model raindrop concentrations. The dots represent samples at azimuthal intervals of ΔAZ along curves that represent the azimuthal profile of Doppler velocity and reflectivity that could be obtained by a WSR–88D if it were to sample continuously. Those curves in the left panels represent super-resolution WSR–88D azimuthal data collection (ΔAZ = 0.5°) and those in the right panels represent current-resolution azimuthal data collection (ΔAZ = 1.0°). The red curves with dots represent Doppler velocity and reflectivity measurements computed from the model tangential velocity and model reflectivity (nonuniform) values. The blue dashed curves with dots represent Doppler velocity and reflectivity measurements based on model tangential velocity values and a uniform reflectivity value of 20 dBZ (the uniform value of 20 dBZ corresponds to the initial concentration of raindrops in the model); the dashed 20 dBZ line represents both the initial reflectivity values and the values after being scanned by the radar. EBW/CD is the ratio of effective radar beamwidth relative to the core diameter of the tornado, Z is height, R is range from the radar, and EL is the radar elevation angle at height Z and range R.

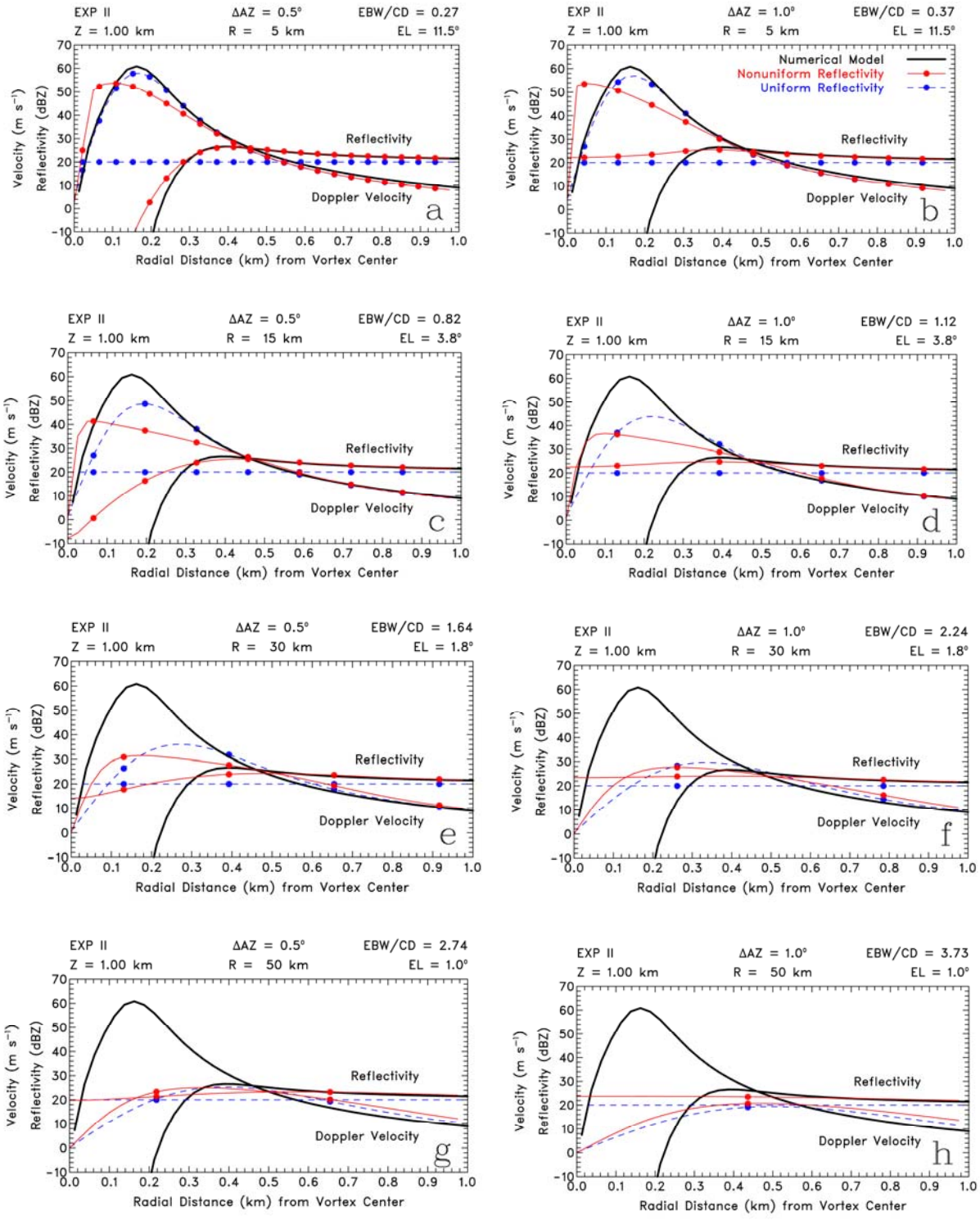

Fig. 2. Same as Fig. 1, except that the results are for Experiment II at ranges of 5, 15, 30, and 50 km. Also, the abscissa and ordinate scales are different.

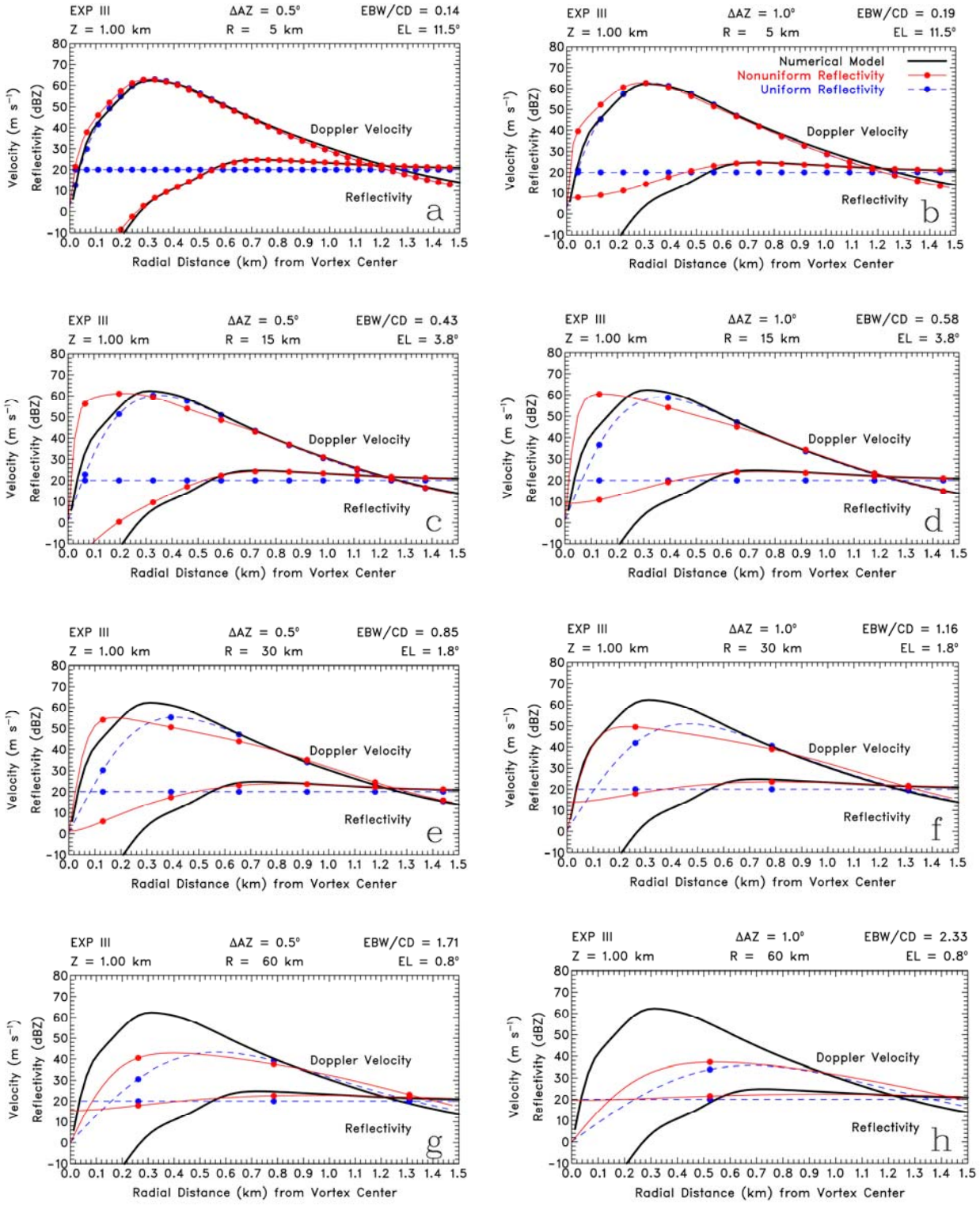

Fig. 3. Same as Fig. 1, except that the results are for Experiment III at ranges of 5, 15, 30, and 60 km. Also, the abscissa and ordinate scales are different.